

## Host Kappa

### Methodology

Host kappa values were estimated using the IRVT approach (Al Atik et al. 2013) for the following GMPEs for a reference  $V_{s30}$  of 760 m/sec: Abrahamson et al. (2014) (ASK14), Boore et al. (2014) (BSSA14), Campbell and Bozorgnia (2014) (CB14), Chiou and Youngs (2014) (CY14), Bindi et al. (2013) (Bindi13), Akkar et al. (2013) (ASB13), and Zhao et al. (2006) (Zhao06).

The IRVT approach relies upon deriving GMPE response spectra-compatible Fourier amplitude spectra (FAS) using inverse random vibration theory (IRVT) as implemented in the computer program STRATA (Kottke and Rathje 2008). Input to STRATA consists of the GMPE response spectra and ground motion duration estimates for the scenarios considered. GMPE host kappa values are estimated using the high-frequency slope of the response spectra-compatible FAS according to the Anderson and Hough (1984) method for short-distance scenarios. To decouple kappa from site amplification effects, the FAS are first divided by the host site amplification factors before estimating host kappa.

As discussed in Al Atik et al. (2013), response spectra with strong high-frequency attenuation such as the Western United States (WUS) spectra are subject to saturation effects resulting from the increased contribution of Fourier amplitudes at lower frequencies to the high-frequency spectral accelerations. This makes it difficult to resolve the FAS at high frequencies (greater than about 30 to 35 Hz for WUS GMPEs) resulting in potentially inaccurate values at these frequencies. Saturation has a more pronounced effect for spectra with stronger high-frequency damping than for those with lower host kappa.

### Host Kappa Values

Host kappa values were estimated for the 7 candidate GMPEs using the IRVT approach for normal faulting scenarios with a dip angle of 50 degrees, for magnitude 5.0, 6.0, and 7.0 and Rx distances of 5, 10, and 20 km on the footwall. These magnitude, distance, and style-of-faulting scenarios were selected because of their significant contribution to the hazard at PVNGS while also limiting the Q attenuation effects on the spectra (short-distance scenarios). Rupture width was calculated according to Wells and Coppersmith (1994) and the hypocenter was assumed to be located at the center of the fault rupture. The depth to top of rupture was calculated according to Chiou and Youngs (2014) as a function of magnitude. Ground motion duration was estimated by adding the source and path durations, which were calculated according to the WUS stochastic model parameters of Campbell (2003) with a stress drop of 100 bars.

The western US (WUS)  $V_s$  profile of Kamai et al. (2013) with a  $V_{s30}$  of 760 m/sec was used as a representative  $V_s$  profile for the host region as shown in Figure 1. Linear site amplification factors for the host  $V_s$  profile were developed using the square-root-impedance (SRI) or quarter wavelength (QWL) method (Boore 2005). Amplification factors were derived at the surface of the profile with respect to the half-space located at a depth of around 9.6 km with  $V_s$  of 3.5 km/sec. Default densities based on

WUS  $V_s$ -density relationships built into the QWL program were used. An angle of incidence at the source of zero degrees was adopted. Figure 2 shows the QWL host site amplification factors.

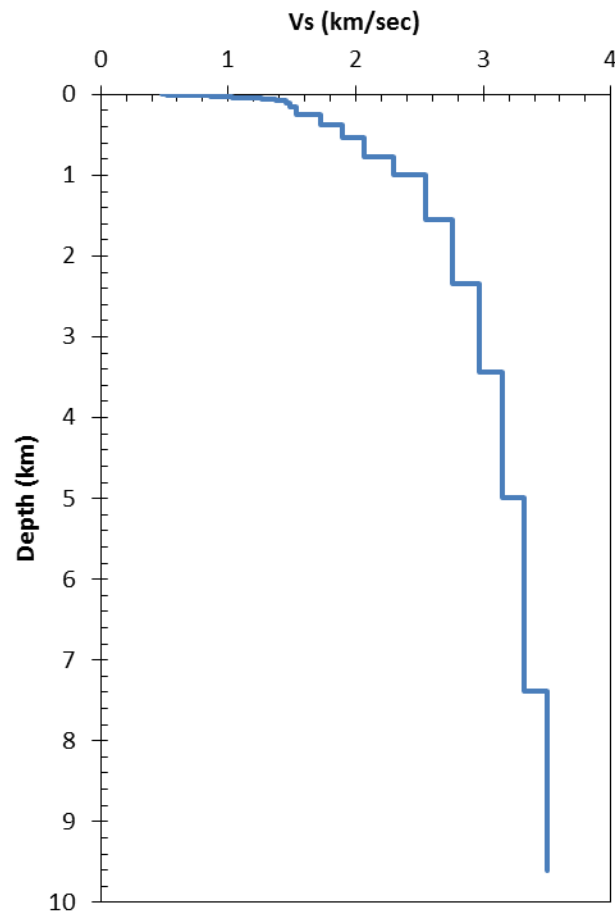


Figure 1. Host  $V_s$  profile with  $V_{s30}$  of 760 m/sec based on Kamai et al. (2013)

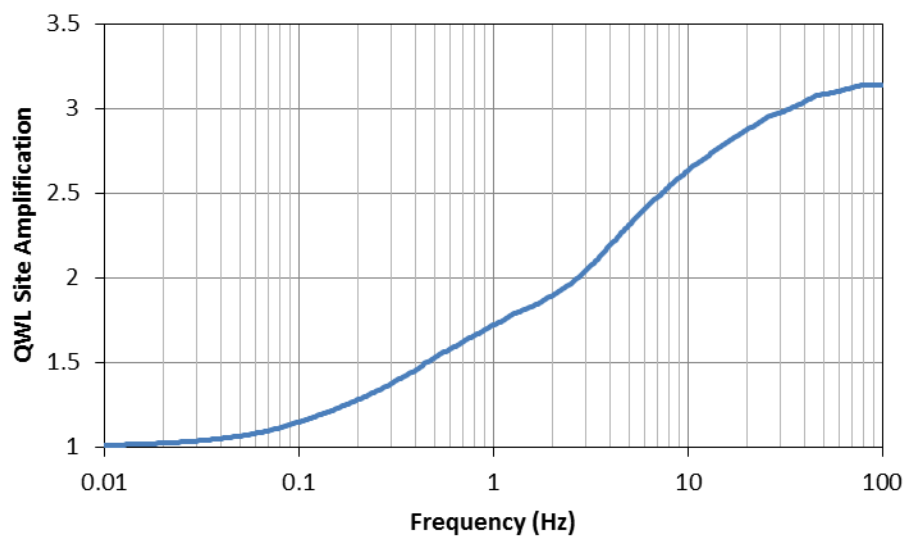


Figure 2. QWL linear site amplification factors for the host  $V_s$  profile with  $V_{s30}$  of 760 m/sec

GMPE response spectra-compatible FAS were derived using the IRVT approach for the 9 scenarios considered and then divided by the host site amplification factors shown in Figure 2 to decouple the site amplification from kappa effects at high frequency. The resulting FAS were inspected to select the start and end frequencies ( $f_1$  and  $f_2$ ) over which  $\log(\text{FAS})$  versus frequency is linear. Kappa for each of the nine scenarios considered (M 5.0, 6.0, and 7.0 and Rx 5, 10, and 20 km) was estimated by fitting the Anderson and Hough (1984) exponential kappa scaling function to the FAS between  $f_1$  and  $f_2$ . Estimated kappa values were averaged for the nine scenarios considered to define the host kappa for 7 candidate GMPEs. Note that kappa derived using the IRVT approach ( $\kappa_1$ ) is not equal to the zero-distance kappa,  $\kappa(0)$ . However, for the short-distance scenarios considered, the anelastic attenuation effects are considered negligible and  $\kappa_1$  approximates  $\kappa(0)$ . Assuming that the source contribution to kappa is negligible,  $\kappa_1$  also approximates  $\kappa_{\text{site}}$ .

Kappa estimates are sensitive to the choice of  $f_1$  and  $f_2$ . Figure 3 shows an example of the effect of different  $f_1$  and  $f_2$  choices on the resulting host kappa estimates for CY14 for the magnitude 6.0 and Rx = 10 km scenario. Figure 3 shows that for 3 different  $f_1$  and  $f_2$  picks,  $\log(\text{FAS})$  versus frequency is linear but the resulting kappa estimates are 0.037, 0.040 and 0.042 sec. Host kappa values for the 7 candidate GMPEs were derived for the best picks of  $f_1$  and  $f_2$ . Figures 4 to 10 show the high-frequency kappa fit to the derived FAS for the 7 candidate GMPEs for the M6.0 and Rx 10 km scenario. Best estimate host kappa values were averaged for each GMPE the 9 scenarios considered and the best estimates are presented in Table 1.

**Table 1. Best estimate host kappa values for the 7 candidate GMPEs for a reference  $V_{s30}$  of 760 m/sec.**

GMPE	ASK14	BSSA14	CB14	CY14	ASB13	Bindi13	Zhao06
Host Kappa (sec)	0.045	0.038	0.037	0.041	0.042	0.045	0.042

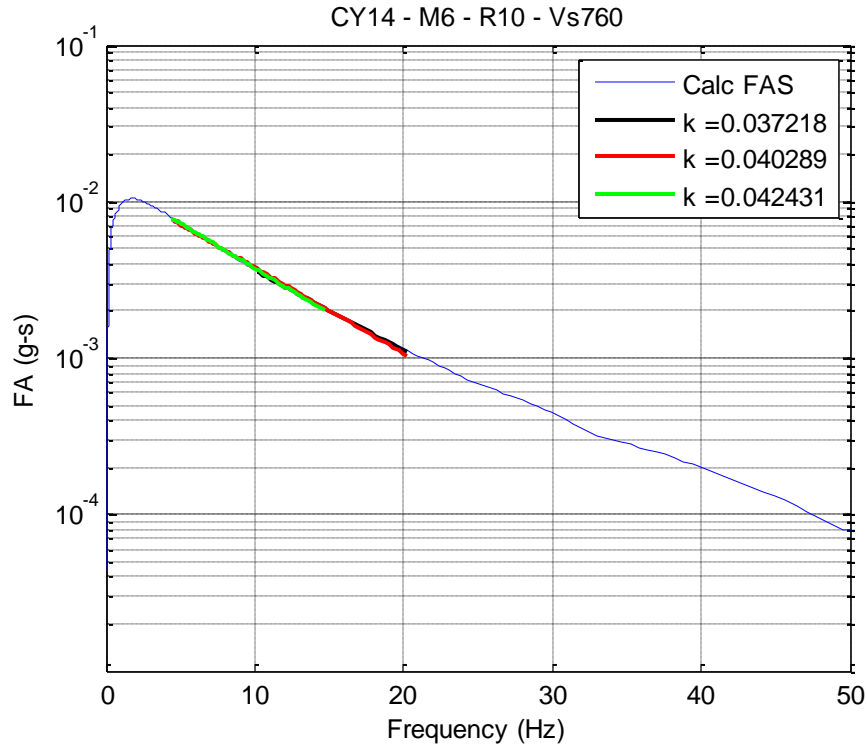


Figure 3. Sensitivity of host kappa estimates to the choice of  $f_1$  and  $f_2$  for CY14 for a scenario with magnitude 6.0 and distance of 10 km

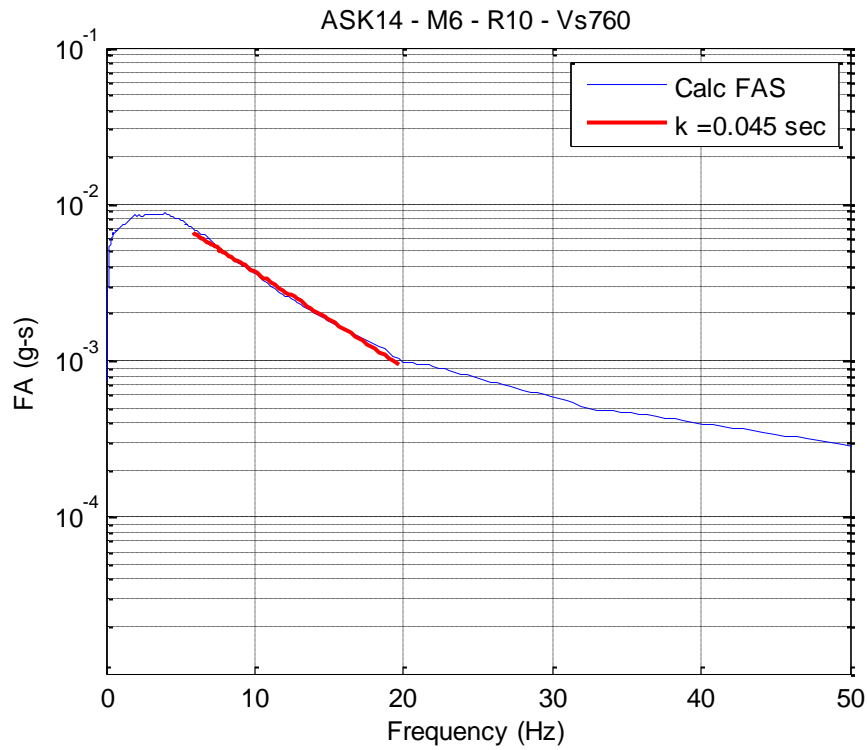


Figure 4. Host kappa value for ASK14 for the M6.0 and  $R_x = 10\text{km}$  scenario

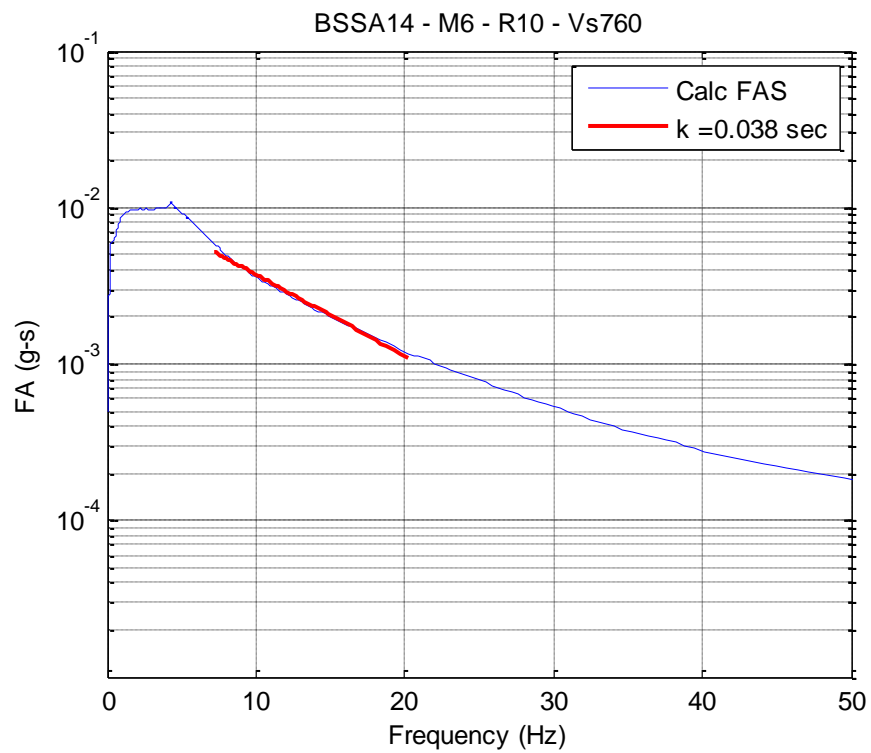


Figure 5. Host kappa value for BSSA14 for the M6.0 and Rx = 10km scenario

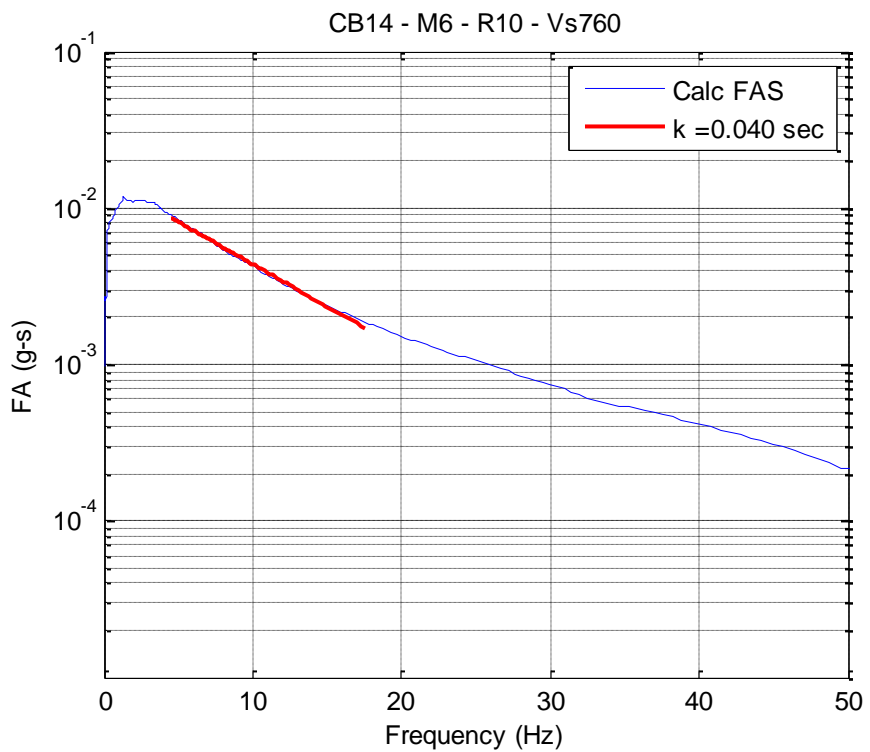


Figure 6. Host kappa value for CB14 for the M6.0 and Rx = 10km scenario

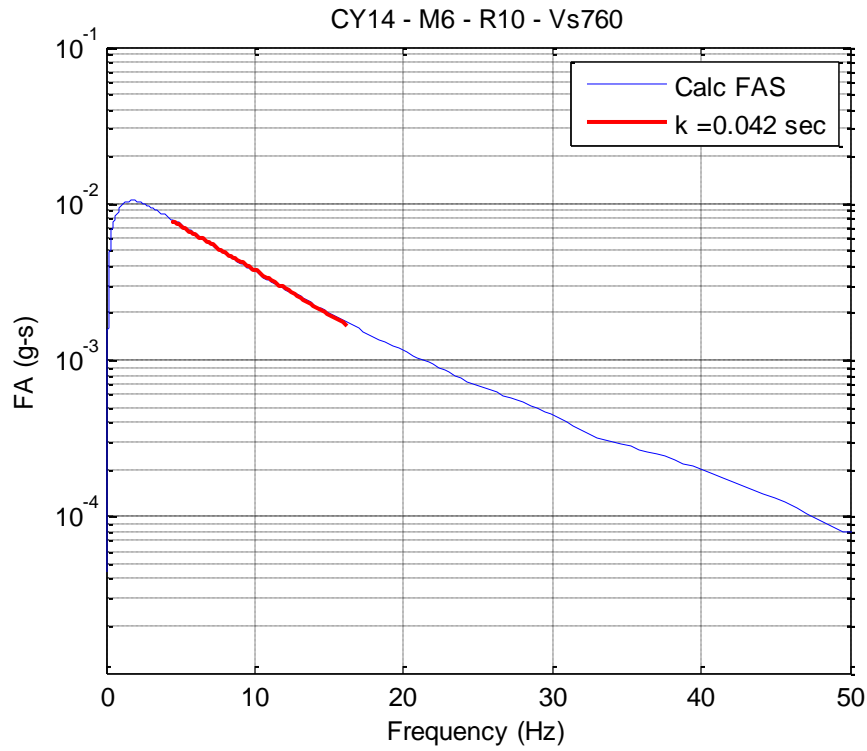


Figure 7. Host kappa value for CY14 for the M6.0 and Rx = 10km scenario

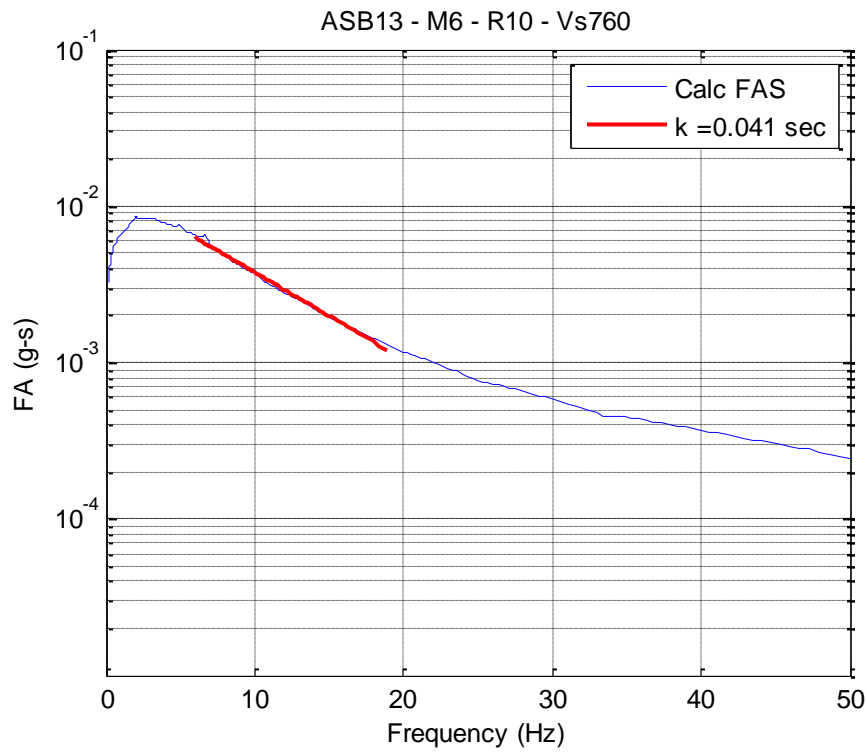


Figure 8. Host kappa value for ASB13 for the M6.0 and Rx = 10km scenario

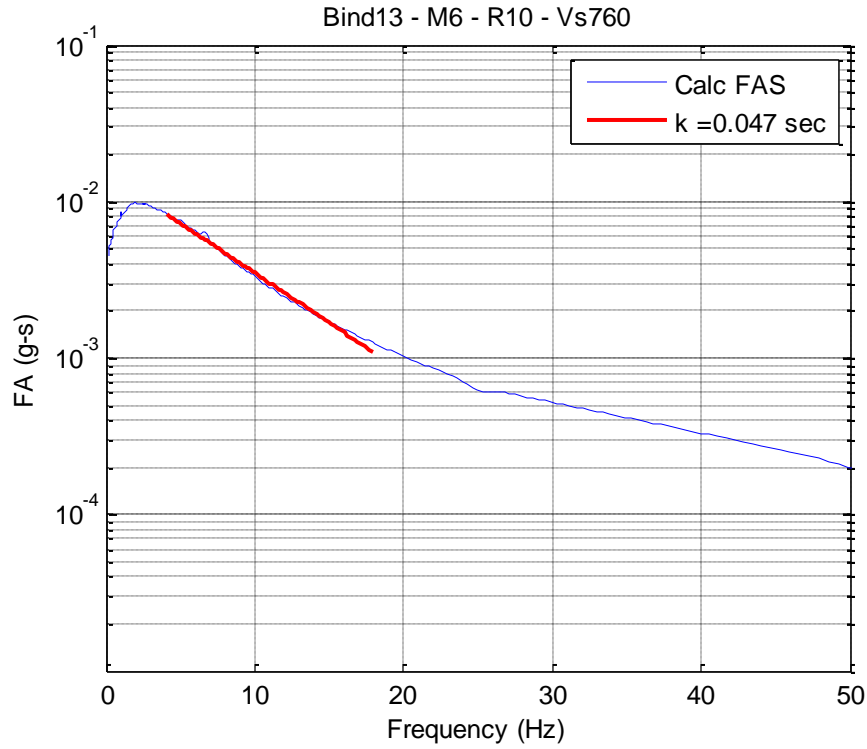


Figure 9. Host kappa value for Bind13 for the M6.0 and Rx = 10km scenario

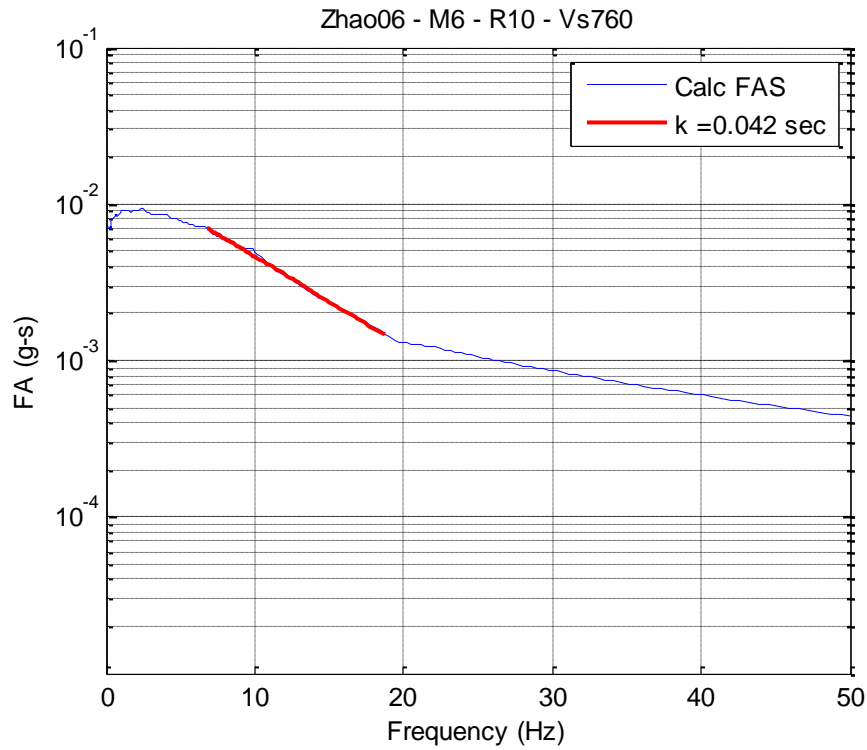


Figure 10. Host kappa value for Zhao06 for the M6.0 and Rx = 10km scenario